Journal of Materials Science & Technology 34 (2018) 2189–2196

Contents lists available at ScienceDirect

Journal of Materials Science & Technology

journal homepage: www.jmst.org

Synthesis of porous carbon spheres derived from lignin through a facile method for high performance supercapacitors

Yuemei Chen [a], Guoxiong Zhang [a], Jingyuan Zhang [a], Haibo Guo [a], Xin Feng [b], Yigang Chen [a,*]

[a] Department of Electronic Information Materials, School of Materials Science and Engineering, Shanghai University, Shanghai, 200444, China
[b] Nano-Science & Technology Research Center, Shanghai University, Shanghai, 200444, China

ARTICLE INFO

Article history:
Received 30 July 2017
Received in revised form 4 November 2017
Accepted 30 December 2017
Available online 31 March 2018

Keywords:
Porous carbon spheres
Supercapacitors
Spray drying
KOH activation

ABSTRACT

Porous carbon spheres (PCS) derived from lignin have been prepared through a facile method and fabricated as electrodes for electric double-layer capacitors. Spherical shaped mixtures of lignosulfonate and crystalized KOH are formed by spray drying of a solution of lignosulfonate and KOH. Activation by KOH is performed at high temperatures along with lignosulfonate carbonization. With an appropriate pore structure, the obtained PCS have a specific surface area of 1372.87 $m^2 g^{-1}$ and show a capacitance of 340 $F g^{-1}$ in 3 M KOH at a current density of 0.5 $A g^{-1}$. Moreover, a symmetric supercapacitor fabricated using the PCS as electrodes show a maximum capacitance of 68.5 $F g^{-1}$, and an energy density of 9.7 $W h kg^{-1}$ at a power density of 250 $W kg^{-1}$. The capacity retention is more than 94.5% after 5000 galvanostatic charge-discharge cycles. The excellent characteristics seem to be ascribed to the pore structures of PCS that have a large specific surface area and a low electrical resistance.

1. Introduction

Due to rapid economic development along with the slather of traditional fossil energy resources, our society faces lots of austere environment problems like global warming and increasingly deteriorating air quality. On this occasion, it is imperative to seek environmentally friendly renewable energy, and to utilize green, efficient energy-storage mechanisms. Currently, supercapacitors, a type of energy-storage devices bridging the power/energy gap between batteries and traditional dielectric capacitors, have attracted considerable attention because of many advantages, such as short charging time, long cycle life, high power density and low cost [1–3]. Regarding the unique characteristics, supercapacitors are widely used for hybrid electronic devices, electrical vehicles, mobile phones, digital cameras and so on [4,5].

According to energy-storage mechanism, supercapacitors can be divided into pseudocapacitors and electrical double layer capacitors (EDLCs). For pseudocapacitors, during the charging and discharging processes, highly reversible Faradic reactions occur at electrode materials, which generally are metal oxides, and in electrolyte of the pseudocapacitors; while for EDLCs there is only pure physical charge accumulation and release on the electrode-electrolyte interface [6,7]. Carbon materials are mostly used as electrode materials in EDLCs for its distinctive properties, including abundance, excellent chemical stability, good electronic conductivity and high specific surface area [8–11].

Although carbon-based electrode materials have many advantages, they have a major drawback of low theoretical capacity and energy density. Therefore, there is a pressing demand to improve the electrochemical properties of carbon materials. Over the years, many studies have been devoted to developing novel structures for carbon-based electrode materials with enhanced electrochemical performance, including 3D hierarchical porous carbon [12,13], 2D carbon nanosheets [14,15] and carbon nanoparticles [16]. These unique structures reduced operating resistance by shortening diffusion paths for mass and charge transport. Meanwhile, some porous structures have increased specific surface area of the electrode materials. Based on the electrical double-layer mechanism, the capacitance of EDLCs mainly relies on the number of the balance charge at the electrode-electrolyte interface. A large surface area is a critical factor for increasing capacitance of EDLCs [1].

Many researchers have reported about creating pores, including macropores, mescropores, and micropores, on carbon-based materials for increasing specific surface areas [17–19]. Macrop-

* Corresponding author.
E-mail address: yigangchen@shu.edu.cn (Y. Chen).

https://doi.org/10.1016/j.jmst.2018.03.010
1005-0302/

ores reserve ions during the charge transport process, thus offering faster ion transport; mescropores facilitate the contact between the electrode material and the electrolyte, thus decreasing contact resistance, and micropores enlarge the specific surface area. However, some micropores whose sizes do not match electrolyte ion sizes may lead to high transport resistance and poor rate performance [20]. In a word, those carbon-based electrode materials with suitable porous structures and high surface areas are ideal for EDLCs.

Many methods involving physical activation and chemical activation were attempted to obtain desirable porous structures. Generally, chemical activation is more effective for creating pores by etching or reacting with carbon [33]. Activators such as KOH, NaCl, $ZnCl_2$, K_2CO_3, and H_3PO_4, etc., mixed with carbon materials or biomass, are placed at high temperatures in an inert atmosphere, where physical and chemical reactions proceed along with carbonization [14,22–24]. Among these activators, KOH is the most widely used activation substance.

From a long-term perspective of development, sustainable biochar has attracted broad attention for its application in supercapacitors. Lignin, one of the ingredients of plant cell wall, is the second largest renewable resource next to cellulose. As a natural aromatic polymer, lignin contains nearly a third of organic carbon on the earth [25,26]. Moreover, numerous lignin derivatives in agricultural waste and paper industry wastewater can be recycled to produce carbon materials. The renewable, environmentally friendly, and cheap lignin-carbon materials could be used to fabricate electrodes and alleviate the demand of fossil when applied in energy-storage devices.

In this study, porous carbon spheres (PCS) derived from lignin have been prepared through a facile method and fabricated as electrodes for EDLCs. Sodium lignosulphonate was the raw material for porous carbon spheres while Potassium hydroxide (KOH) was the activating agent. Spherical shaped mixtures of lignosulfonate and crystalized KOH were formed by spray drying of a solution of lignosulfonate and KOH. Spray drying is a facile and rapid way for drying chemicals in aqueous solutions, and the method makes the chemicals to keep the shape of spherical droplets. Activation occurred in the presence of KOH at high temperatures during lignosulfonate carbonization. As will be seen, with appropriate pore structure, the obtained PCS have a specific surface area of 1372.87 $m^2 g^{-1}$. The excellent characteristics seem to be ascribed to the pore structure that increases the specific surface area and reduces resistance of the PCS-based electrode materials. Thus, the low-cost renewable lignin-derived PCS synthesized through a facile route are the ideal candidate for electrode materials of supercapacitors and other energy-storage devices.

2. Experimental

2.1. Materials

Sodium lignosulphonate was purchased from Aladdin Industrial Corporation, Shanghai, China, and was used as carbon source for synthesizing porous carbon spheres. KOH (of A.R. grade) and concentrated HCl (of A.R. grade) were purchased from Shanghai Sinopharm Chemical Reagent Company, China. Acetylene black (99.9%), polytetrafluoroethylene (PTFE, 50%) and nickel foams were purchased from Tiyuan Liyuan Lithium-ion Battery Technology Center (co., LTD.).

2.2. Preparation of porous carbon spheres

Preparation of porous carbon spheres (PCS) were prepared through five simple and effective steps. First, sodium lignosulphonate and KOH at the mass ratio of 3:1 were dissolved in deionized water to form a solution of 5% mass fraction. Second, the solution was transferred into a spray dryer to dry, and turned into a dark khaki spherical-shaped mixture of lignosulfonate-KOH. Third, the mixture was heated in a tube furnace in nitrogen atmosphere at 700 °C for 2 h with a heating rate of 3 °C min^{-1} for carbonization. Fourth, the carbonized sample was cooled down to room temperature, and washed with 1 M HCl solution under magnetic stirring for 12 h to neutralize alkali as well as to remove other impurities. Finally, the carbonized sample was washed with deionized water for several times until the wash water has neutral pH; then dried in an oven at 80 °C for 24 h. The carbonized sample is denoted as PCS. In comparison, the sample prepared in the same way but without KOH is denoted as CS.

2.3. Physical characterization

The morphology of PCS was investigated by scanning electron microscopy (SEM, JEOL LTD JSM-7500F) and high-resolution transmission electron microscopy (HRTEM, JEOL JEM-2100F). To analyze the structure form of PCS, powder X-ray diffraction analysis (XRD, Rigaku D/max-2550) was carried out using the Cu*K*α radiation source (λ = 0.154 nm). Raman spectra (with the wavenumber range of 500–3000 cm^{-1}) were used to study the molecular structure. Nitrogen adsorption and desorption isotherms were recorded using the BK122WTA analyzer (JWGB). The specific surface area was calculated by the Brunauer-Emmett-Teller (BET) model, and the pore-size distribution was obtained using nitrogen desorption data via the Barrett-Joyner-Halenda (BJH) model.

2.4. Electrochemical characterization

The electrochemical performance of the PCS electrode materials was measured in both three-electrode system and two-electrode system (a supercapacitor device) using a CHI660E electrochemical workstation. For the test in the three-electrode system, the electrolyte was a 3 M KOH aqueous solution; the counter electrode was a platinum foil, and reference electrode was saturated calomel electrode (SCE). As for the working electrode, the PCS powder, acetylene black, and PTFE binder were mixed to form slurry with a mass ratio of 8:1:1, then the slurry was brush-coated onto a 1 cm × 1 cm nickel-foam current collector and dried at 80 °C overnight in an oven. Afterwards, the nickel foam was pressed with a pressure of 10 MPa to form the working electrode. The active mass of PCS in each electrode was about 5 mg. The electrochemical properties were investigated by electrochemical impedance spectroscopy (EIS), cycle voltammetry (CV), and galvanostatic charge-discharge (GCD) profile. The specific capacitance of the PCS working electrode was calculated from the GCD profile using the equation:

$$C = \frac{I\Delta t}{m\Delta V} \quad (1)$$

where C (unit: F g^{-1}) is the specific capacitance of the electrode, I (A) is the constant current within the discharge time Δt (s), m (g) is the mass of PCS on electrode, and ΔV (V) is the voltage change in the discharge process.

For the test in the two-electrode system, the procedure of preparing the electrodes was the same as that in the three-electrode system except that the nickel foam was altered to a circular shape (Φ 15 mm), hence circular electrodes were used instead of square ones. Two almost identical circular electrodes as positive and negative electrodes were packaged in 2016-type electrode-shell with a porous nonwoven cloth separator and 3 M KOH aqueous solution as the electrolyte to fabricate symmetric supercapacitors. The mass of PCS in this supercapacitor was about 10 mg. The specific

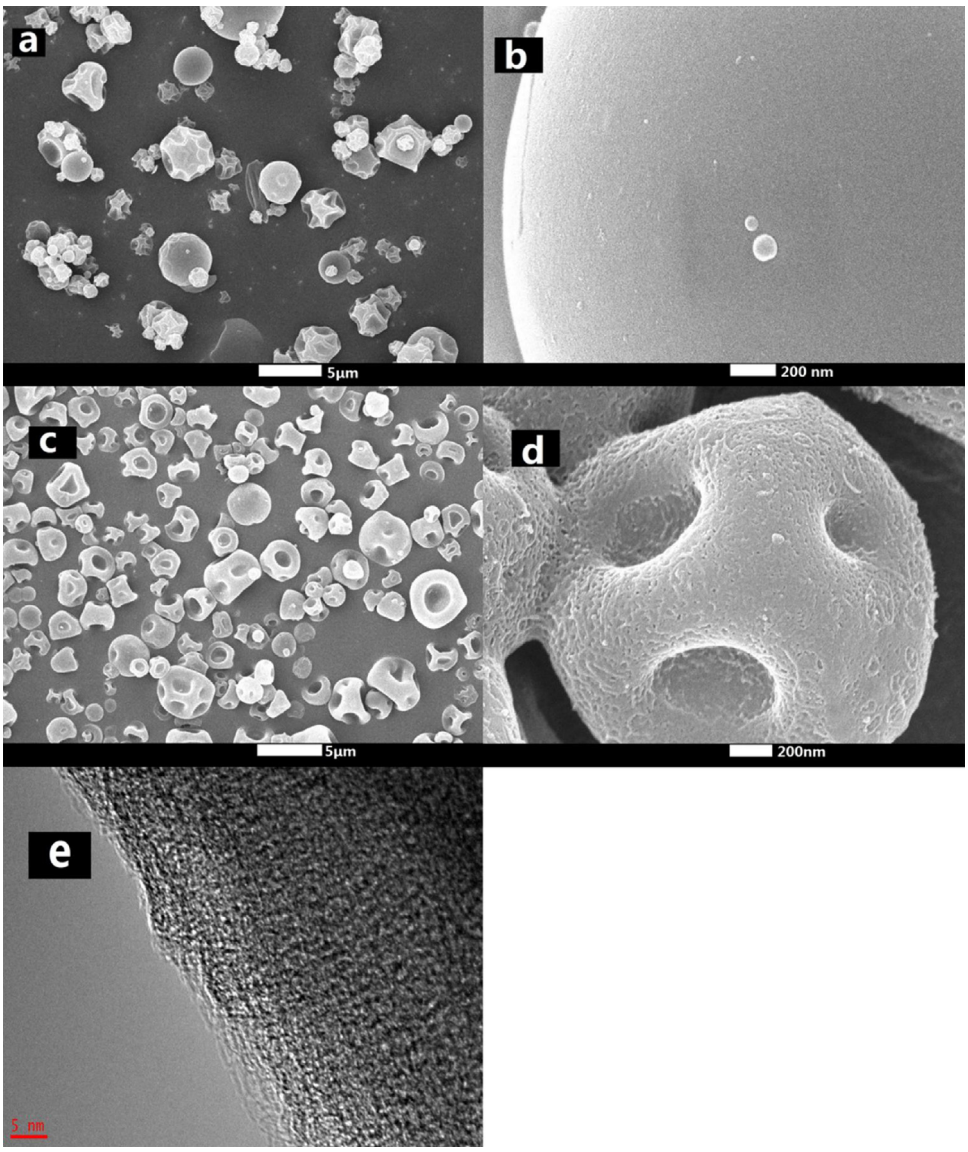

Fig. 1. Morphology images of CS (a, b) and PCS (c, d,e).

capacitance of the symmetric supercapacitor was calculated from the equation:

$$C_s = \frac{I\Delta t}{(m_1 + m_2)\Delta V} \quad (2)$$

where C_s ($F\,g^{-1}$) is the specific capacitance of symmetric supercapacitor, I (A) is the constant current within the discharge time Δt (s), m_1, m_2 (g) are the mass of PCS on two electrodes, respectively, and ΔV (V) is the voltage change in the discharge process. The energy density and power density of PCS symmetric supercapacitor were calculated from the equation:

$$E = \frac{C_s\ \Delta V^2}{2} \quad (3)$$

$$P = \frac{E}{\Delta t} \quad (4)$$

where C_s ($F\,g^{-1}$) is the specific capacitance of symmetric supercapacitor, E ($W\,h\,kg^{-1}$), P ($W\,kg^{-1}$) are the energy density and power density, respectively; C_s ($F\,g^{-1}$), ΔV (V), Δt (s) are the specific capacitance, the voltage change in the discharge process and the discharge time, respectively. In addition, cycle stability tests of the PCS-based electrode were carried out on a LAND battery program-controlled test system (LAND Co. Ltd.)

3. Results and discussion

3.1. Material characterization

Fig. 1(a) shows that the synthesized CS is comprised of irregular spheres with either smooth or wrinkled surfaces. This microstructure is mainly attributed to spay drying process, in which the solution was transformed into minute droplets and dried immediately, becoming a spherical precursor. After the precursor pyrolyzes, the spherical structure is retained, but some wrinkles appear as a result of polycondensation at high temperatures in the carbonization process. As shown in Fig. 1(b), the magnified view of a carbon sphere shows that there are no pores in the surface. From Fig. 1(c), it can be seen that the PCS have many severe dents on their surfaces, a phenomenon probably due to the removal of the KOH or part of the precursor in the rinsing process. Moreover, abundant micropores and mesopores are observed on the surface of the PCS in the high-magnification image (Fig. 1(d)) and fringe of a PCS particle in the HRTEM image (Fig. 1(e)). These pores should have

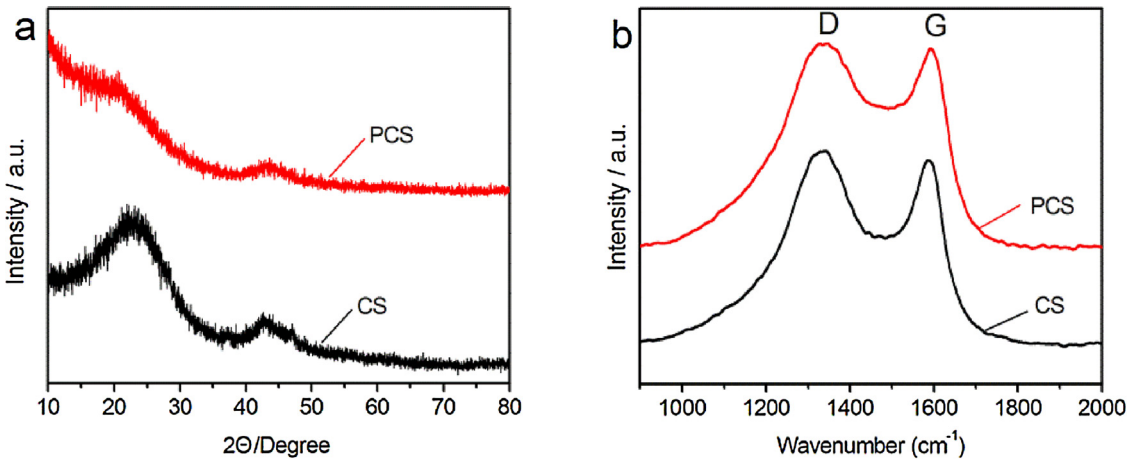

Fig. 2. XRD pattern of the PCS and CS (a); Raman spectra of PCS and CS (b).

been formed in the etching process by KOH. The reactions between KOH and the carbonized precursor proceed as follows (Eqs. (5)–(8)) [12,27].

$$KOH + 2C \rightarrow 2K + 3H_2 + 2K_2CO_3 \quad (5)$$

$$K_2CO_3 \rightarrow K_2O + CO_2 \quad (6)$$

$$K_2CO_3 \rightarrow 2C + 2K_2O \quad (7)$$

$$K_2O + C \rightarrow 2K + CO \quad (8)$$

Meanwhile, the consumption of carbon and the escape of the CO_2 and CO gases result in the abundant pores.

The sunken surface and abundant pores render the PCS a large specific surface area. Besides, the novel structure of the PCS not only facilitates the contact between the electrode material and the electrolyte, but also offers a short path for transport of electrolyte ions. Therefore, electrodes made of the PCS are expected to be beneficial to improving electrochemical performance of supercapacitors.

Fig. 2(a) shows the XRD spectra of the PCS and CS. Both materials exhibit two broad scattering peaks at 22.3° and 43.8°, corresponding to the (100) and (002) reflections of carbon, respectively, revealing that they are amorphous [28]. The diffraction pattern of the PCS is characterized by a higher intensity in the small-angle region, and two broader scattering peaks than that of the CS, indicating the presence of more micropores in the PCS [29,30]. Furthermore, the structure characteristics of the samples are also

Table 1
The pore properties of PCS and CS.

	S_{BET} [$m^2\ g^{-1}$]	V_{pore}[$m^3\ g^{-1}$]	D_{aver}[nm]
Sample PCS	1590	0.89	2.59
Sample CS	663	0.33	2.14

investigated by Raman spectroscopy, and the results are shown in Fig. 2(b). There are two peaks located at around 1344 cm^{-1} (D band, defect and disorder) and 1595 cm^{-1} (G band, graphitic) in the Raman spectra of both PCS and CS. The relative intensity ratio of D band and G band (I_D/I_G) reflects crystallization degree of carbon materials [31]. The ratios of I_D/I_G for the PCS and CS are estimated to be 1.26 and 1.14, respectively. The larger I_D/I_G ratio for the PCS confirms a more disordered structure, which might be correlated to its highly porous structure [32]. The characterization results demonstrate that the PCS possesses a large amount of pores after being etched by KOH, and the etching process causes a certain degree of damage to the perfect graphitic phase and increases the disorder degree of the carbon materials.

The porosity characteristics of the samples are further described by N_2 adsorption-desorption isotherms in Fig. 3(a). It can be seen that CS displays the IUPAC type-I adsorption-desorption isotherm with major N_2 adsorption at low relative pressures (P/P_0), due to the existence of micropores. But, the isotherm curve of PCS exhibits combined type-I and type-IV features, showing strong N_2 adsorption at low relative pressures ($P/P_0 \sim 0$) and an evident hysteresis

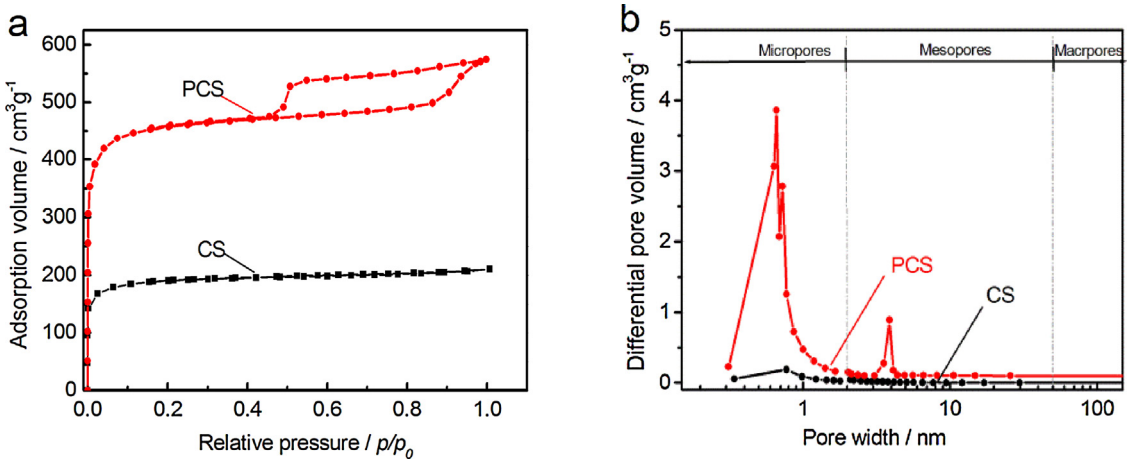

Fig. 3. N_2 adsorption-desorption isotherms of PCS and CS (a); pore size distribution of PCS and CS (b).

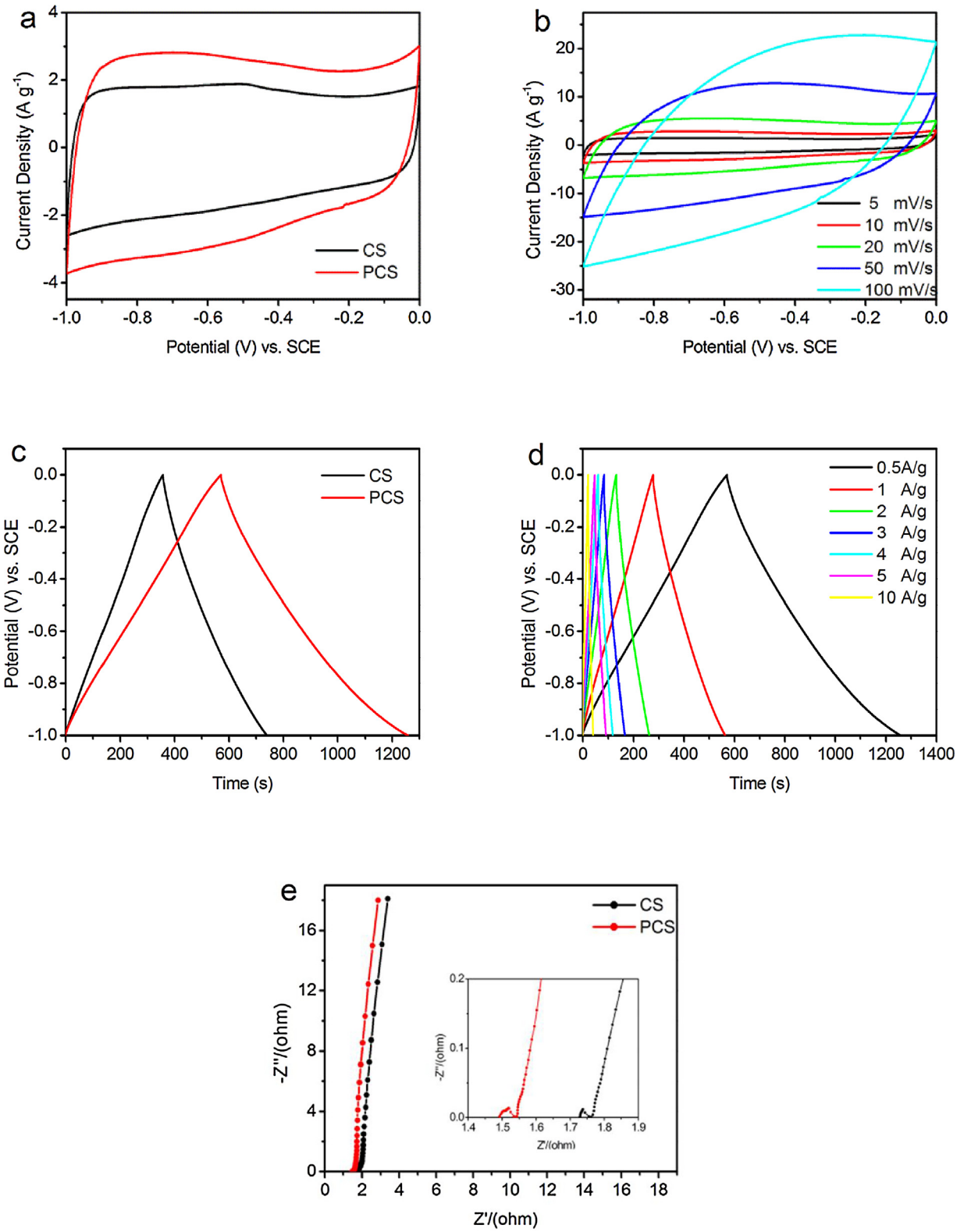

Fig. 4. CV curves of CS and PCS at 10 mV s^{-1} scanning rate (a); CV curves of PCS at different scan rates (b); galvanostatic charge-discharge curves of CS and PCS at 0.5 A/g current density (c); galvanostatic charge-discharge curves of PCS at different current densities (d); electrochemical impedance spectroscopy (EIS) of CS and PCS (e).

loop at high relative pressures (P/P_0 from 0.5-1). The result indicates that there are abundant micropores and mesopores in the PCS. The pore size distribution of PCS and CS are illustrated in Fig. 3(b). For the PCS, it is clear that the micropores' diameter ranges from 0.3 to 1.6 nm, and peaks at about 0.7 nm; while the mesopores' diameter ranges from 2 to 25 nm, and peaks at about 4 nm. As for CS, the curve has hardly any fluctuation, except for a small peak at about 0.8 nm. Table 1 presents pore-specific properties of PCS and CS. One sees from Table that the specific surface area (1590 m^2 g^{-1}) and total pore volume (0.89 m^3 g^{-1}) of PCS are both larger than those of CS

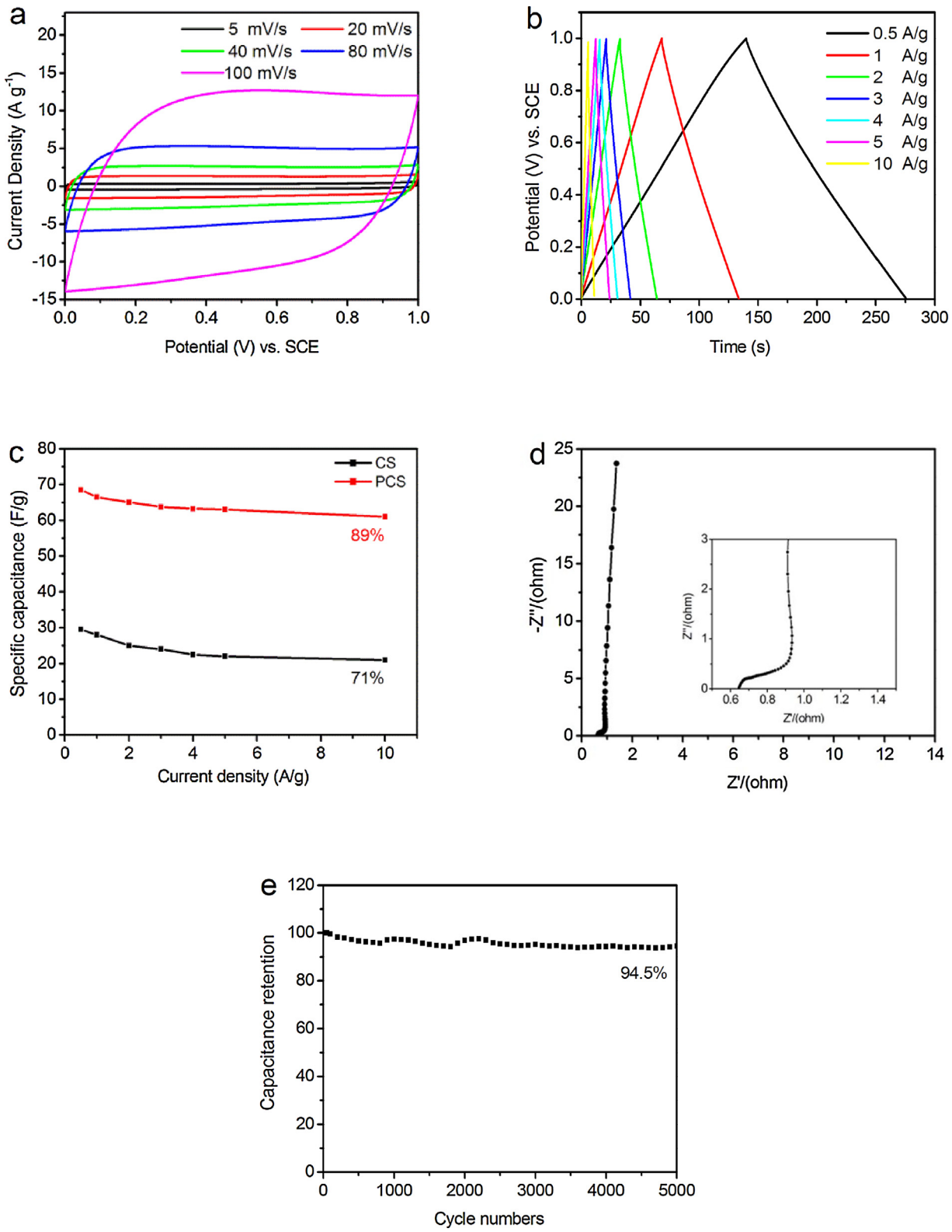

Fig. 5. CV curves of PCS based symmetric supercapacitor at different scan rates (a); GCD curves of PCS based symmetric supercapacitor at different current densities (b); the specific capacitance of PCS and CS based symmetric supercapacitor at different current densities (c); electrochemical impedance spectroscopy of PCS based symmetric supercapacitor (d); cycle stability of PCS based symmetric supercapacitor at a current density of 4 A/g for 5000 cycles (e).

whose specific surface area is 663 $m^2 g^{-1}$ and total pore volume is 0.33 $m^3 g^{-1}$. The excellent porosity properties of PCS are believed to be capable of attracting more charges and offering faster ion transport, thus better improving the electrochemical performance of supercapacitors than CS.

3.2. Electrochemical characterization

3.2.1. Three electrode analysis

Fig. 4(a) shows the CV curves of CS and PCS at a scan rate of 10 mV s^{-1} from −1.0 to 0 V in a 3 M KOH aqueous electrolyte. Both

curves have a quasi-rectangular shape, a characteristic of typical electric double layer capacitance. The larger enclosed area by the CV curves of the PCS indicates that the PCS has a higher capacitance than the CS, and the improvement should be due to its suitable porous structures that are beneficial for charge accumulation and fast ionic transport [33]. The CV curves of the PCS at different scan rates (ranging from 5 to 100 mV s^{-1}) are showed in Fig. 4(b). The shape of the curves remains nearly rectangular with slight deformation that increases with the scan rate, indicating a good rate capability and good electrochemical performance of the PCS electrode for EDLC.

The GCD curves of CS and PCS at a current density of 0.5 A g^{-1} between −1 and 0 V in Fig. 4(c) show that the discharging time of PCS is much longer than CS, signifying higher specific capacitance of PCS electrode, as calculated from Eq. (1). The result is consistent with CV measurements, and it might be due to the larger effective specific surface area and pore volume of PCS. Fig. 4(d) shows GCD curves of PCS at different current densities (0.5, 1, 2, 3, 4, 5, 10 A g^{-1}). All the curves have symmetric triangular shapes. For the voltage window from −1 to 0 V, the specific capacitances of the PCS electrode are 345, 293, 270, 268, 255, 250, 245 F g^{-1} for the current densities from 0.5 to 10 A g^{-1}, respectively. The specific capacitance decreases slowly with the increasing of current density, and still retains 71% capacitance at a high current density of 10 A g^{-1}, indicating that the PCS electrode has excellent energy-storage capability.

The impedance properties of PCS and CS are presented by Nyquist plots (Fig. 4e). The two plots are basically similar, both consisting of a semi-circle in the high frequency region and an almost vertical line at the low frequency region, exhibiting the typical feature of electrodes materials for EDLC. The interception of the semicircle on X-axis represents equivalent series resistance (R_S), and the R_S are 1.73 Ω and 1.49 Ω for CS and PCS, respectively. The reason for the smaller resistance of the PCS might be that it has more abundant pores that promote the contact area between the PCS and the electrolyte. The diameter of the semicircle represents the charge-transfer resistance (R_{CT}), and the short diameters for PCS and CS indicate that they both have fast charge transfer. The slope of the nearly vertical line is associated with ion diffusion, and a higher slope corresponds to a smaller diffusion resistance. The slopes of the nearly vertical lines for CS and PCS are the same. In short, the PCS has smaller electrode-electrolyte contact resistance and shorter ion transfer pathway than the CS, thus is a better electrode material for EDLC.

3.2.2. Two electrode analysis

In order to further verify the energy-storage capacity of the PCS electrode materials for EDLC, a symmetric supercapacitor is assembled using the PCS as electrodes to test its electrochemical characteristics in a two-electrode system. Fig. 5a shows CV curves of PCS-based symmetric supercapacitor at different scan rates ranging from 5 to 200 mV s^{-1}, and all the curves are of rectangular shapes even when the scanning rate is 200 mV s^{-1}, implying good rate capability of the PCS-based symmetric supercapacitor. The GCD curves of the PCS-based supercapacitor show symmetrical triangular shapes at different current densities (Fig. 5(b)). The specific capacitances of the symmetric supercapacitor are 68.5, 66.5, 65, 63.7, 63.2, 63.0, and 61.0 F g^{-1} at current densities of 0.5, 1, 2, 3, 4, 5, and 10 A g^{-1}, respectively. The capacitance decreases slowly with the current density, and still retains 89% capacitance at a high current density of 10 A g^{-1}. This demonstrates the excellent rapid charge and discharge capacity at high current densities, as further shown in Fig. 5(c). For comparison, the capacitive performance of the CS in the two-electrode system is shown in the same figure. The specific capacitances of the CS-based symmetric supercapacitor are 29.5, 28, 25, 24, 22.5, 22, and 61 F g^{-1} at current densities of 0.5, 1, 2, 3, 4, 5, and 10 A g^{-1}, respectively, and retains 71% capacitance at current density of 10 A g^{-1}. The better performance of the PBC-based supercapacitor might be due to the PCS's novel structure, which facilitates contact between the electrode material's surface and the electrolyte. For impedance analysis, the Nyquist plot of the symmetric supercapacitor (Fig. 5(d)) shows a nearly vertical line at low frequencies, and the small value of interception on the *x*-axis (0.64 Ω), indicating that the PCS electrode materials have ideal impedance properties for supercapacitors and other electrochemical energy-storage devices. Moreover, cycle life tests of the PCS-based symmetric supercapacitor are carried out on LAND battery program-controlled test system at a current density of 4 A g^{-1} in a 3 M KOH solution. The fluctuation of the specific capacitance versus cycle number is showed in Fig. 5e. After 5000 cycles, the supercapacitor retains about 94.5% capacitance of the initial value, exhibiting an outstanding cycle stability of the PCS-based electrode for practical applications.

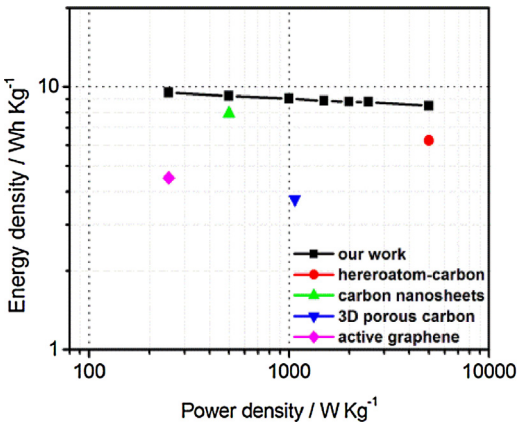

Fig. 6. Ragone plot of PCS based symmetric supercapacitor.

Fig. 6 shows the Ragone plot of the PCS-based supercapacitor. The supercapacitor possesses an energy density of 9.7 W h kg^{-1} at a power density of 250 W kg^{-1}, and when the power density is 5000 W kg^{-1}, the device achieves a power density of 8.47 W h kg^{-1} which exceeds many supercapacitors based on other forms carbon of electrode materials, such as heteroatom doped carbon, carbon nanosheets, 3D porous carbon, active graphene [13,22,34,35] and commercial devices [36]. These excellent electrochemical performances demonstrate that the novel PCS electrode material is very promising for EDLCs.

4. Conclusion

In summary, porous carbon spheres for high performance supercapacitors have been prepared through spray drying and carbonization with lignosulfonate as the carbon source and KOH as the activator. Because of its novel porous structure, the obtained sample has a high specific surface area of 1372.87 m^2 g^{-1}, and shows a capacitance of 340 F g^{-1} in 3 M KOH at a current density of 0.5 A g^{-1}. Furthermore, a PCS-based symmetric supercapacitor is fabricated, and the device displays a good energy-storage capacity that has a capacitance of 68.5 F g^{-1} at a current density of 0.5 A g^{-1}. The capacity retention is higher than 94% after 5000 galvanostatic charge-discharge cycles, indicating good electrochemical stability. The excellent characteristics might be ascribed to its spherical morphology with suitable micro/mesoporous structures and high effective surface areas. The low-cost renewable lignin-derived porous carbon spheres are the ideal candidate for electrode materials of large-scale supercapacitors and other electrochemical energy-storage devices.

Acknowledgment

This study is primarily supported by Shanghai Eastern-scholar program.

References

[1] Y. Zhai, Y. Dou, D. Zhao, P.F. Fulvio, R.T. Mayes, S. Dai, Adv. Mater. 23 (2011) 4828–4850.
[2] X. Zhao, B.M. Sanchez, P.J. Dobson, P.S. Grant, Nanoscale 3 (2011) 839–855.
[3] H. Jiang, P.S. Lee, C. Li, Energy Environ. Sci. 6 (2013) 41–53.
[4] L.L. Zhang, X.S. Zhao, Chem. Soc. Rev. 38 (2009) 2520–2531.
[5] Z. Yang, J. Zhang, M.C.W. Kintner-Meyer, X. Lu, D. Choi, J.P. Lemmon, J. Liu, Chem. Rev. 111 (2011) 3577–3613.
[6] F. Cao, G.X. Pan, X.H. Xia, P.S. Tang, H.F. Chen, J. Power Sources 264 (2014) 161–167.
[7] F. Beguin, V. Presser, A. Balducci, E. Frackowiak, Adv. Mater. 26 (2014) 2219–2251, 2283.
[8] G. Wang, L. Zhang, J. Zhang, Chem. Soc. Rev. 41 (2012) 797–828.
[9] C.M.A. Parlett, K. Wilson, A.F. Lee, Chem. Soc. Rev. 42 (2013) 3876–3893.
[10] Y. Li, Z.Y. Fu, B.L. Su, Adv. Funct. Mater. 22 (2012) 4634–4667.
[11] L. Dai, D.W. Chang, J.B. Baek, W. Lu, Small 8 (2012) 1130–1166.
[12] L. Qie, W. Chen, H. Xu, X. Xiong, Y. Jiang, F. Zou, X. Hu, Y. Xin, Z. Zhang, Y. Huang, Energy Environ. Sci. 6 (2013) 2497–2504.
[13] W. Zhang, H. Lin, Z. Lin, J. Yin, H. Lu, D. Liu, M. Zhao, Chemsuschem 8 (2015) 2114–2122.
[14] J. Hou, C. Cao, F. Idrees, X. Ma, Acs Nano 9 (2015) 2556–2564.
[15] Y. Fang, Y. Lv, R. Che, H. Wu, X. Zhang, D. Gu, G. Zheng, D. Zhao, J. Am. Chem. Soc. 135 (2013) 1524–1530.
[16] Y.H. Zhao, M.X. Liu, L.H. Gan, X.M. Ma, D.Z. Zhu, Z.J. Xu, L.W. Chen, Energy Fuels 28 (2014) 1561–1568.
[17] L. Pang, B. Zou, X. Han, L. Cao, W. Wang, Y. Guo, Mater. Lett. 184 (2016) 88–91.
[18] Y. Lv, L. Gan, M. Liu, W. Xiong, Z. Xu, D. Zhu, D.S. Wright, J. Power Sources 209 (2012) 152–157.
[19] Y. Qiao, H. Wang, X. Zhang, P. Jia, T. Shen, X. Hao, Y. Tang, X. Wang, W. Gao, L. Kong, Mater. Lett. 184 (2016) 252–256.
[20] H.J. Liu, J. Wang, C.X. Wang, Y.Y. Xia, Adv. Energy Mater. 1 (2011) 1101–1108.
[22] Y. Wang, Y. Liu, W. Liu, G. Zhang, G. Liu, H. Chen, J.L. Yang, J. Alloys Compd. 677 (2016) 105–111.
[23] X. He, Z. Liu, H. Ma, N. Zhang, M. Yu, M. Wu, Microporous Mesoporous Mater. 236 (2016) 134–140.
[24] F. Sun, J. Gao, X. Liu, X. Pi, Y. Yang, S. Wu, Appl. Surf. Sci. 387 (2016) 857–863.
[25] J. Zakzeski, P.C.A. Bruijnincx, A.L. Jongerius, B.M. Weckhuysen, Chem. Rev. 110 (2010) 3552–3599.
[26] K.L. Wang, M. Xu, Y. Gu, Z.R. Gu, Q.H. Fan, J. Power Sources 332 (2016) 180–186.
[27] M. Armandi, B. Bonelli, F. Geobaldo, E. Garrone, Microporous Mesoporous Mat. 132 (2010) 414–420.
[28] W. Chen, H. Zhang, Y. Huang, W. Wang, J. Mater. Chem. 20 (2010) 4773–4775.
[29] W. Qian, F. Sun, Y. Xu, L. Qiu, C. Liu, S. Wang, F. Yan, Energy Environ. Sci. 7 (2014) 379–386.
[30] H. Feng, H. Hu, H. Dong, Y. Xiao, Y. Cai, B. Lei, Y. Liu, M. Zheng, J. Power Sources 302 (2016) 164–173.
[31] X.G. Yang, C. Li, W. Wang, B.J. Yang, S.Y. Zhang, Y.T. Qian, Chem. Commun. (2004) 342–343.
[32] Q. Wang, J. Yan, Y. Wang, T. Wei, M. Zhang, X. Jing, Z. Fan, Carbon 67 (2014) 119–127.
[33] J. Wang, S. Kaskel, J. Mater. Chem. 22 (2012) 23710–23725.
[34] Y.Q. Zhao, M. Lu, P.Y. Tao, Y.J. Zhang, X.T. Gong, Z. Yang, G.Q. Zhang, H.L. Li, J. Power Sources 307 (2016) 391–400.
[35] Y. Zhu, S. Murali, M.D. Stoller, K.J. Ganesh, W. Cai, P.J. Ferreira, A. Pirkle, R.M. Wallace, K.A. Cychosz, M. Thommes, D. Su, E.A. Stach, R.S. Ruoff, Science 332 (2011) 1537–1541.
[36] Y. Gogotsi, P. Simon, Science 334 (2011) 917–918.